Response to the comments of Reviewer 1

First of all, we would like to thank the anonymous reviewer for the careful review and valuable suggestions. We carefully revised the manuscript following the suggestions. Hereby we give a point-by-point reply to address the comments. In this document, the words in *italics are the reviewers' comments*, the words in blue are the modifications we have made in the revision, and others are our responses.

Q1: *The work aims to study the sea ice freeboard in areas around the Antarctic peninsula. Improved sea ice surface topography is a useful product and can be implemented in other studies, such as ice drift product development and climate studies. The manuscript is reasonably well written and mostly easy to follow. Some of the terminology is at times somewhat confusing. There are a great many figures in the manuscript, could some perhaps be moved to supplementary information.*

A1: We thank the reviewer for the positive comment about our research. We have carefully revised the manuscript based on the following comments.

Q2: *In the abstract the terms sea ice DEM, i.e. snow freeboard is introduced. How does this relate to the sea ice topography? Why is the sea ice DEM not = sea ice and snow freeboard? How is the air-ocean-ice system related to the sea ice topography? The statement as it stands right now is a bit challenging to interpret.*

A2: We apologize for any confusion caused by the term "snow freeboard." In this paper, when referring to sea ice DEMs, we actually mean the total freeboard, which includes both the ice freeboard and the thickness of the snow layer. Therefore, whenever we mention "sea ice elevation," it actually means the total freeboard. In the revised version, we have explicitly defined sea ice DEMs as total freeboard (snow+ice). We have made corrections by replacing "snow freeboard" with "total freeboard" and updated the term "sea ice elevation" to "total freeboard" throughout the manuscript, including both the text and figures, to ensure clarity and consistency.

In the revision, we have restated the sentence in the abstract: The total freeboard (snow+ice) is crucial for reflecting sea ice dynamics and interpreting the geophysical environments of polar oceans.

In the Introduction section, we have included detailed explanations about how the air-ocean-ice system is related to sea ice topography:

The sea ice topography plays a crucial role in reflecting sea ice dynamics and interactions within the air-ocean-ice system. It showcases the spatial distribution of distinct surface features such as snow dunes (Trujillo et al., 2016; Iacozza and Barber, 1999) and deformed ice (Haas et al., 1999; Petty et al., 2016), which are impacted by the forces from winds and currents. Moreover, the atmospheric drag coefficient over sea ice, which is topography-dependent, is an important parameter for understanding interactions at the ice-atmosphere boundary (Garbrecht et al., 2002; Castellani et al., 2014).

Castellani, G., Lüpkes, C., Hendricks, S., and Gerdes, R.: Variability of Arctic sea-ice topography and its impact on the atmospheric surface drag, J. Geophys. Res.: Oceans, 119, 6743–6762, https://doi.org/10.1002/2013JC009712, 2014.

Garbrecht, T., Lüpkes, C., Hartmann, J., and Wolff, M.: Atmospheric drag coefficients over sea ice–validation of a parameterisation concept, Tellus A: Dynamic Meteorology and Oceanography, 54, 205–219, https://doi.org/10.3402/tellusa.v54i2.12129, 2002.

Haas, C., Quanhua, L., and Thomas, M.: Retrieval of Antarctic sea-ice pressure ridge frequencies from ERS SAR imagery by means of in situ laser profiling and usage of a neural network, International Journal of Remote Sensing, 20, 3111–3123, 1999.

Iacozza, J. and Barber, D. G.: An examination of the distribution of snow on sea-ice, Atmosphere-Ocean, 37, 21–51, https://doi.org/10.1080/07055900.199 1999.

Petty, A. A., Tsamados, M. C., Kurtz, N. T., Farrell, S. L., Newman, T., Harbeck, J. P., Feltham, D. L., and Richter-Menge, J. A.: Characterizing Arctic sea ice topography using high-resolution IceBridge data, The Cryosphere, 10, 1161–1179, https://doi.org/10.5194/tc-10- 1161-2016, 2016.

Trujillo, E., Leonard, K., Maksym, T., and Lehning, M.: Changes in snow distribution and surface topography following a snowstorm on Antarctic sea ice, Journal of Geophysical Research: Earth Surface, 121, 2172–2191, https://doi.org/10.1002/2016JF003893, 2016.

Q3: *R21. If we assume that the DEM is snow freeboard, should it then be assumed that no penetration if the snow is possible?*

A3: The term "sea ice DEMs" refers to the total freeboard, which is ice freeboard plus snow depth. We have modified it to 'total freeboard' throughout the manuscript.

Q4: *R22-23. Please elaborate how this product is essential for assessing the impact of climate change on sea ice.*

A4: We have modified in the introduction: Moreover, the DEM (i.e., total freeboard) can be converted to thickness with the knowledge of snow depth and the assumed values of snow, ice, and seawater densities (Kwok and Kacimi, 2018). Estimating sea ice thickness over time offers valuable insights into the overall stability of sea ice in the changing climate.

Q5: *R58-59. How can the DEM help separate the different ice types?*

A5: In R58-59, we do not intend to imply that the DEM can help separate different ice types. Rather, we mean that sea ice types can serve as prior knowledge for generating DEM from InSAR. The InSAR-derived height represents the elevation of the InSAR phase center, which is not necessarily at the snow-air surface due to radar penetration. The depth of penetration varies depending on the ice type, with sea ice having lower salinity and being covered by dry snow allowing for deeper penetration compared to ice with higher salinity and wet snow cover. To ensure accurate sea ice DEM retrieval, we proposed first classifying the sea ice into small-penetration and larger-penetration conditions, followed by retrieving the sea ice DEM using standard InSAR processing and the proposed TLPV model for each ice type, respectively.

In the revision, we have rewritten the sentence for clarity:

The initial step involves the development of a random forest classifier using specific SAR features to categorize sea ice into two groups: small-penetration condition ice (SPI) and large-penetration condition ice (LPI), based on the penetration depth of microwaves. Subsequently, a sea ice DEM is created for each ice type. In the case of SPI, standard InSAR processing is applied to determine the elevation. For LPI, a novel inversion algorithm is proposed to estimate the parameters of the developed TLPV model (Huang et at., 2021). This allows for correcting penetration bias in the InSAR signal over LPI, resulting in an accurate retrieval of total freeboard. We validate the proposed method against the photogrammetric DEM from the IceBridge aircraft. A root-mean-square error (RMSE) of $0.26\,\mathrm{m}$ between the derived DEM and reference data indicates an improved accuracy in total freeboard retrieval.

Q6: *R67. What is meant with Ice Chart here? An operational ice charts such as those provided by the ice services. What is meant is explained on R108. This one of the terminology words introduced it the introduction that gets explained later in the manuscript. This terminology should either be removed from the introduction or needs to be explained here.*

A6: We have removed the terminology and revised the sentences as:

...in sea ice classes obtained from an operational product from the U.S. National Ice Center.

Q7: *R91. Perhaps state how the denoising is done then why it's useful/essential to do so here.*

A7: The SAR-measured backscattering intensity ($\sigma_{\mathrm{measure}}$) containing additive thermal noise can be denoted as

$$\sigma_{\mathrm{measure}} =< (S_{\mathrm{denoised}} + N) \times (S_{\mathrm{denoised}} + N)^* > \tag{1}$$

where S_{denoised} is the noise-subtracted backscattering amplitude, and N is the additive thermal noise. Considering S_{denoised} and N to be uncorrelated, the noise-subtracted backscattering intensity can be obtained from the following simple equation (Nghiem et al., 1995)

$$\sigma_{\mathrm{denoised}} = \sigma_{\mathrm{measure}} - NESZ \tag{2}$$

where $NESZ$ is the noise floor (i.e., the noise equivalent sigma zero (NESZ)), and all terms are in the linear domain.

The TanDEM-X product contains a set of polynomial coefficients that describe the NESZ pattern for each polarization along the range direction (Eineder et al., 2008) for both the TanDEM-X (TDX) and TerraSAR-X (TSX) images. An example of the calculated $NESZ$ is shown in Fig.1 in dB scale. By converting to the linear scale, the $\sigma_{\mathrm{denoised}}$ can be calculated by subtracting $NESZ$ from the $\sigma_{\mathrm{measure}}$. We calculated the NESZ pattern for each SAR acquisition and employed Eq. 2 to generate denoised backscattering intensities for the different polarizations (i.e., HH, VV, Pauli-1 (HH+VV), and Pauli-2 (HH-VV)) from the TSX image. Note that for Pauli-1 and Pauli-2, we use the average $NESZ$ between HH and VV channels.

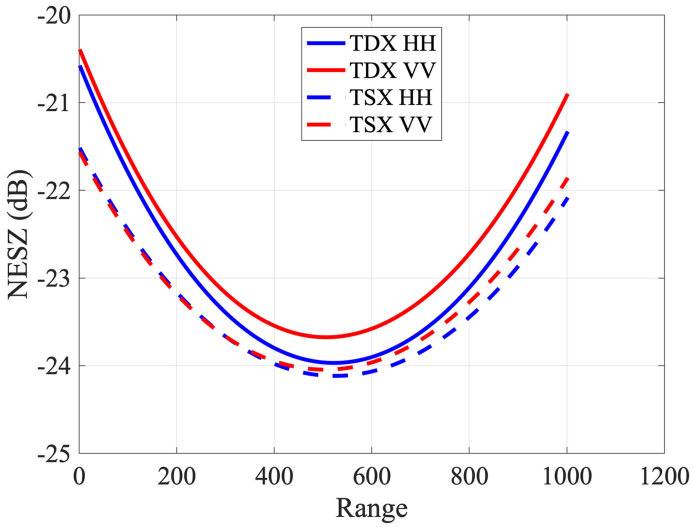

Fig. 1: NESZ patterns for one TanDEM-X acquisition (Scene No.1, see Fig.2 in the paper) as an example.

In the revision, we have added the above description in the supplementary information.

Thermal noise can contaminate the SAR backscattering intensity. Removing the thermal noise allows for a better representation of sea ice features from SAR image, which is crucial for ice classification. The denoised SAR backscattering intensity was input as the features for the random forest classifier in Section 3.1.

In the revision, we have added the usefulness of the denoising processing:

The backscattering intensity σ_{measure} of the images includes additive thermal noise, which can be described by the noise equivalent sigma zero (NESZ) and assumed to be uncorrelated with the signal (Nghiem et al., 1995). Removing the thermal noise allows for a better representation of sea ice features, which is crucial for ice classification. We denoised backscattering intensities for the different polarizations (i.e., HH, VV, Pauli-1 (HH+VV), and Pauli-2 (HH-VV)) by subtracting the noise equivalent sigma zero (NESZ) from the σ_{measure}, see details in the supplementary information.

Nghiem, S., Kwok, R., Yueh, S., and Drinkwater, M.: Polarimetric signatures of sea ice: 2. Experimental observations, J. Geophys. Res.:490 Oceans, 100, 13 681–13 698, https://doi.org/10.1080/08843759508947700, 1995.

Eineder, M., Fritz, T., Mittermayer, J., Roth, A., Boerner, E., & Breit, H. (2008). TerraSAR-X ground segment, basic product specification docu-ment (Tech. Rep.). Cluster Applied Remote Sensing (CAF).

Q8: *Table 1. One of the datasets (R5) has a higher HoA. Does this affect the results presented here?*

A8: The HoA (h_a) is the height of ambiguity determined by the specific InSAR configuration such as the radar wavelength, orbit height, incidence angle, and baseline. h_a is used in converting InSAR phase (ϕ_γ) into height (h_{InSAR}) through $h_{\text{InSAR}} = \frac{\phi_\gamma}{2\pi} h_a$.

However, a larger HoA (ranging from 40 to 42 meters) will elevate the uncertainty in InSAR-derived height. This uncertainty (σ_h) can be estimated by (Madsen and Zebker, 1998):

$$\sigma_h = \frac{h_a}{2\pi} \sigma_{\Delta_\phi}$$

where σ_{Δ_ϕ} is the phase noise, which can be expressed as a function of the interferometric coherence (γ_{InSAR}) and the independent number of looks (N_L) (Rosen et al., 2000):

$$\sigma^2_{\Delta_\phi} = \frac{1}{2N_L} \frac{1 - \gamma^2_{\text{InSAR}}}{\gamma^2_{\text{InSAR}}}$$

The simulated σ_h to the variations in h_a and γ_{InSAR} is illustrated in Fig. 2. At the $\gamma_{\text{InSAR}} = 0.75$, σ_h increases from $0.35\,\text{m}$ to $0.48\,\text{m}$ corresponding to h_a ranging from $30\,\text{m}$ to $42\,\text{m}$. Across the studied region, both the mean and median values of γ_{InSAR} are around 0.75. Consequently, in the case of R5, the larger h_a induces a relatively larger average uncertainty (around $0.13\,\text{m}$) in the derived InSAR height (h_{InSAR}) compared to the smallest h_a InSAR configuration in our dataset.

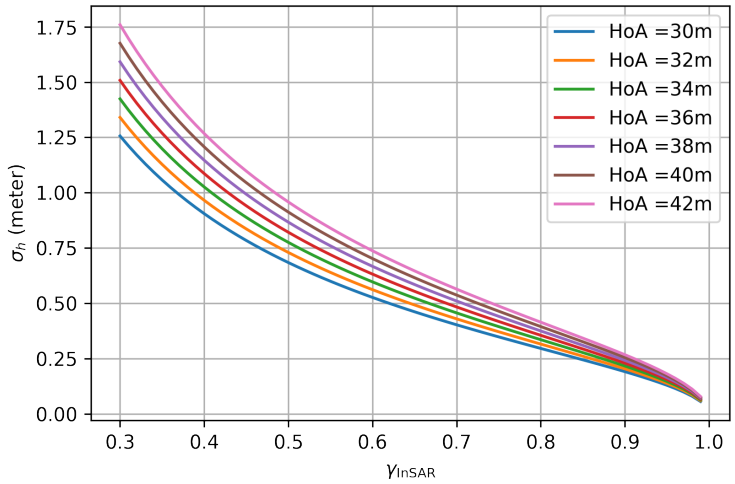

Fig. 2: Simulation of σ_h to variations in h_a and γ_{InSAR}. In our case $N_L = 73$.

In the revision, we have added the above analyses in the supplementary information.

Madsen, S. N. and Zebker, H. A.: Imaging Radar Interferometry, in: Principles and Applications of Imaging Radar, Manual of Remote Sensing, 3rd Edn., John Wiley & Sons, New York, 2, 359380, 1998.

Rosen, P. A., Hensley, S., Joughin, I. R., Li, F. K., Madsen, S. N., Rodriguez, E., and Goldstein, R. M.: Synthetic aperture radar interferometry, P. IEEE, 88, 333–382, https://doi.org/10.1109/5.838084, 2000.

Q9: *R111. The spatial resolution of the Ice Charts is 10 x 10 km. How wide are the SAR images used? Will more than a few pixels be comparable between the Ice Charts and the SAR images?*

A9: In Figures 13-15, we present the sea ice topography variation (total freeboard and roughness from SAR) at $100\,\mathrm{km}$ intervals. Specifically, we selected the SAR pixels at each $100\,\mathrm{km}$ distance and computed statistics for their total freeboard and roughness. The resolution of each SAR pixel is $500 \times 500\,\mathrm{m}$. Given that the Ice Charts have a spatial resolution of $\sim 10 \times 10\,\mathrm{km}$, we directly plotted the values from them. Consequently, in the first columns, you can observe approximately 10 points from the Ice Charts at every $100\,\mathrm{km}$ interval.

There are more than a few SAR pixels compared to a single Ice Chart pixel. We do not down-sample the SAR results to match the Ice Charts resolution, since our objective is to generate a high-resolution (sub-kilometer) sea ice DEM and explore its role in understanding the spatial variation of sea ice topography (as detailed in Section 4.2). It is also essential to clarify that we utilized Ice Charts data merely as an external information source in interpreting the topographic variation. However, we did not employ the Ice Charts for validating the proposed method. For validation purposes, we conducted pixel-by-pixel comparisons using co-registered DMS data, which were down-sampled to the same resolution level as the SAR result.

Q10: *Figure 3, 4 and 7. The schematic in Figure 3 in itself is good but it's challenging to understand if perhaps Figure 4 is step 1, and if so why this isn't stated in Figure 4. Please indicate how these 3 flow charts are interconnected. It appears as if Step 1 is in part explained in Figure 4 but it's unclear as more information than the TanDEM-X SAR images are used as input data? And the classification map at the end of Figure 4 appears to perhaps be the first box in Step 1. Figure 7 appears to be an explanation of the top right box in Step 2 in Figure 3. Please clarify these flow charts.*

A10: Figure 3 provides a detailed explanation of the training process for the sea ice classifier in Step 1. Figure 4 elaborates on the PolInSAR height retrieval module in Step 2, including inverting the proposed TLPV model to generate h_{mod}. During the training and validation phases of both the sea ice classifier and the PolInSAR height retrieval module, DMS DEMs were input as reference data. With the trained classifier and the module, the two-step method was applied to TanDEM-X SAR images together with AMSR level-3 snow depth measurements as input. We have merged the three figures into one for clarification:

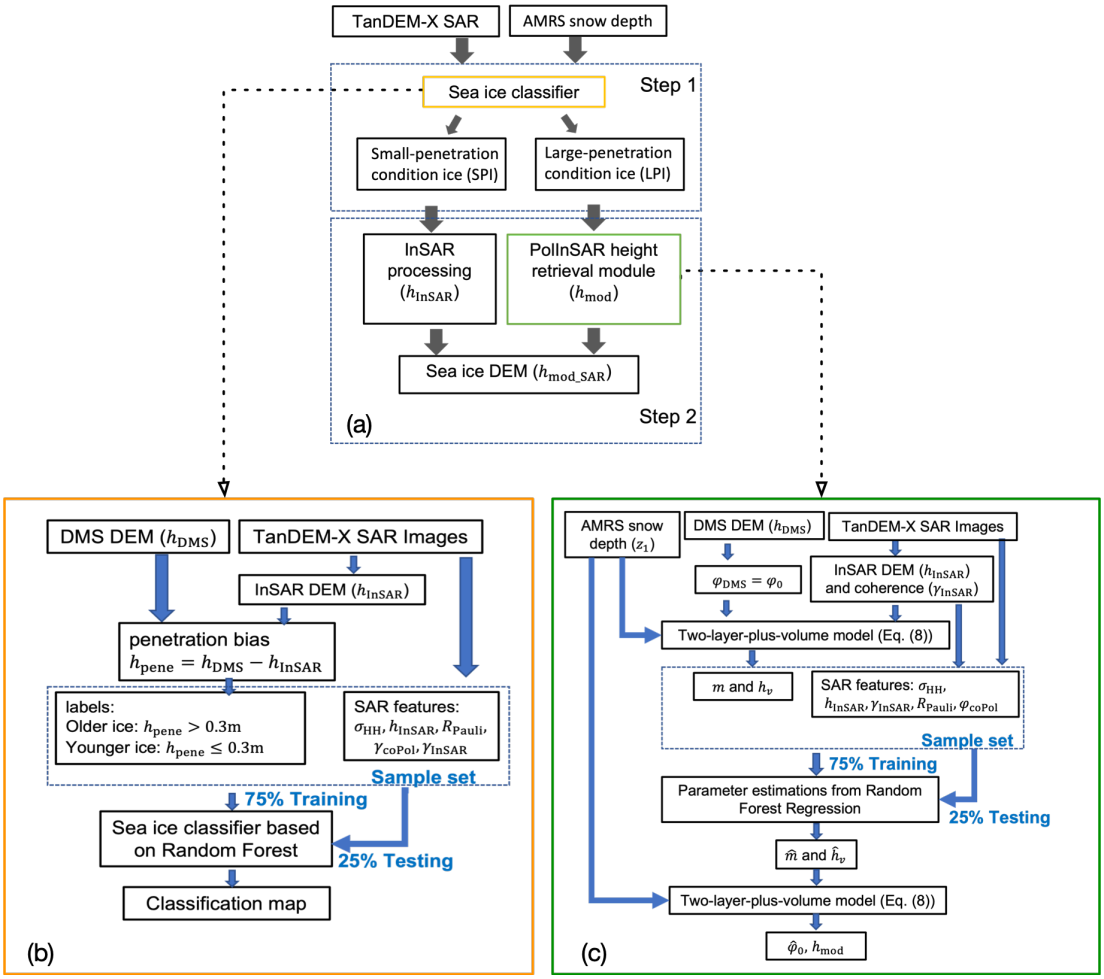

Fig. 3: (a) The proposed two-step approach for sea ice DEM retrieval. (b) The details (training and validation) of the sea ice classifier and (c) the PolInSAR height retrieval module.

The above flowchart has been added to the revision.

Q11: *R180-184. Are some parameters more important for one of specific ice types? Or is the importance level presented in Fig 5 universal?*

A11: The Gini importance is a metric used in a random forest classifier to measure the relative importance of each feature in making classification decisions. It is calculated based on the decrease in Gini impurity that each feature contributes to the overall model.

The computed Gini importance is not inherently specific to a particular class or ice type. Instead, it represents the relative importance of features in making overall classification decisions within the context of the entire dataset. Therefore, the importance level determined by Gini importance is not specific to individual ice types but reflects the significance of features for the classifier's overall predictive performance across all classes (i.e., SPI and LPI).

Q12: *Figure 9. Some of the leads appear to have a light blue color, not the same as for the YI. Why is that? Which ice type do they represent? They appear to in 1, 2 and 3 have the highest E. What is the unit E? Does a low SNR perhaps get mistaken as a thick sea ice? Perhaps could a noise analysis remove erroneous values?*

A12: We apologize for the confusion. The light blue is the color of the base map used for plotting. During InSAR processing, we excluded pixels with an InSAR coherence less than 0.3, setting their values to NaN. When plotted, NaN values are rendered as void areas, showing the color of the base map. Since pixels with low InSAR coherence often correspond to water areas, it appears that all leads and water areas are colored in light blue. The SAR backscattering intensities in the water area mostly range below -19dB. Note that the system noise level of TanDEM-X is around -19 to -26dB. These pixels exhibiting low SNR induce significant uncertainty in InSAR processing. As a result, we have excluded these regions (i.e., open water leads) from

further analyses. In the revision, we have changed the color of the base map to transparent (white) and added a statement in the caption: The void pixels in the second and third columns represent water areas excluded from processing due to $\gamma_{\mathrm{InSAR}} < 0.3$.

In the third column of Fig. 9, the label is a vertically printed "m" which stands for meter, not "E." This column represents the derived sea ice DEM (total freeboard, in the unit of meter) using the proposed two-step method. Scenes 1, 2, and 3 near the Antarctic Peninsula exhibit higher total freeboard. The analysis of the higher freeboard and the spatial variation along the transect are provided in Section 4.2. In the revision, we have changed the colorbar's label to meter for clarity.

Q13: *Figure 11. In the top, upper middle and bottom figures, it appears as if the SAR estimates are underestimating the high and low peaks. Is this a resolution issue? Or is there some other explanation behind this?*

A13: In the postprocessing, we geocoded the DMS DEM into the SAR coordinate and down-sampled the DMS DEM into the same resolution as the SAR pixel size ($10 \times 10\,\mathrm{m}$ in the ground range and azimuth). Therefore, resolution is not likely the cause of underestimation.

One factor contributing to the underestimation of total freeboard could be the assumption of a constant average snow depth over one SAR scene (spatial coverage of $50 \times 19\,\mathrm{km}$). The constant average snow depth is an input parameter z_1 in the TLPV model. In our methodology, we assume this snow depth remains uniform across one SAR image due to the limited spatial resolution of available snow measurements (AMSR Level-3 data with a resolution of $12.5\,\mathrm{km}$). However, this uniformity may lead to an underestimation of snow depth in high-peak areas such as ridges, consequently resulting in an underestimation of the total freeboard. Our prior study (Huang et al., 2021) demonstrated a mean difference of $0.31\,\mathrm{m}$ in the derived total freeboard due to snow depth variations from 0.05 to $0.75\,\mathrm{m}$ over Scene No.1, highlighting the impact on peak estimation. In the future, it would be interesting to adapt the proposed total freeboard retrieval method over the test sites co-locating with available high-resolution snow depth measurements.

Another factor that could potentially lead to the underestimation of high and low-peak areas is the residual shift between the SAR and DMS images. Although we carefully co-registered the four SAR scenes with the DMS data, the co-registration can not be perfect. In the process, we divided the entire overlapped transect into small segments (each corresponding to $100 \times 1000\,\mathrm{m}$). We assumed the same drift location over one segment and no rotation; thus, only one shift vector was used for co-registration over each segment. This could result in small residual shifts when the ice floes or features do not drift at the same velocity or involve rotations. For high and low-pixel ice features with narrow sizes covering one or a few pixels, even 1-2 pixels of residual shifts could lead to some loss or mismatched information of the ice structure from the SAR images. The mismatched SAR images input into the proposed model could result in underestimation when compared with the total freeboard from the DMS DEM.

We have added the above text in a new Section Discussion in the revision.

Huang, L., Fischer, G., and Hajnsek, I.: Antarctic snow-covered sea ice topography derivation from TanDEM-X using polarimetric SAR455 interferometry, The Cryosphere, 15, 5323–5344, https://doi.org/10.5194/tc-15-5323-2021, 2021.

Q14: *Figure 12. This figure could perhaps be moved to supplementary information as it doesn't add much to the understanding of the results. It's very challenging to see the elevations, if kept perhaps make the SAR images a lot larger?*

A14: In the revision, we have enlarged the size of Fig. 12. However, due to the ratio of the width and length of the transects, the enlarged plot occupies a full page, so we decided to move it to supplementary information.

Q15: *Figure 13, 14, 15. Consider coloring the y-axis and the color used in the plot the same color for easier interpretation of the information contained within the figures. Add a legend to the two rightmost columns, to explain what the blue and the orange represents.*

A15: In the revision, we have improved the first column in Fig. 13-15 by incorporating visualizations of ice concentration for each ice type (MYI, FYI, and TI) from the Ice Charts, instead of only showing the "average ice type" as in the previous manuscript version. We have utilized a consistent colormap (same as Fig.16) to represent each ice type. We have included a legend for clarity in the second and third columns as suggested.

Note that these updated plots are primarily for improved visual comparison between the Ice Charts and the SAR results, with no alterations to the main observations or conclusions within the Section Results.

The updated Fig13-15 are given below:

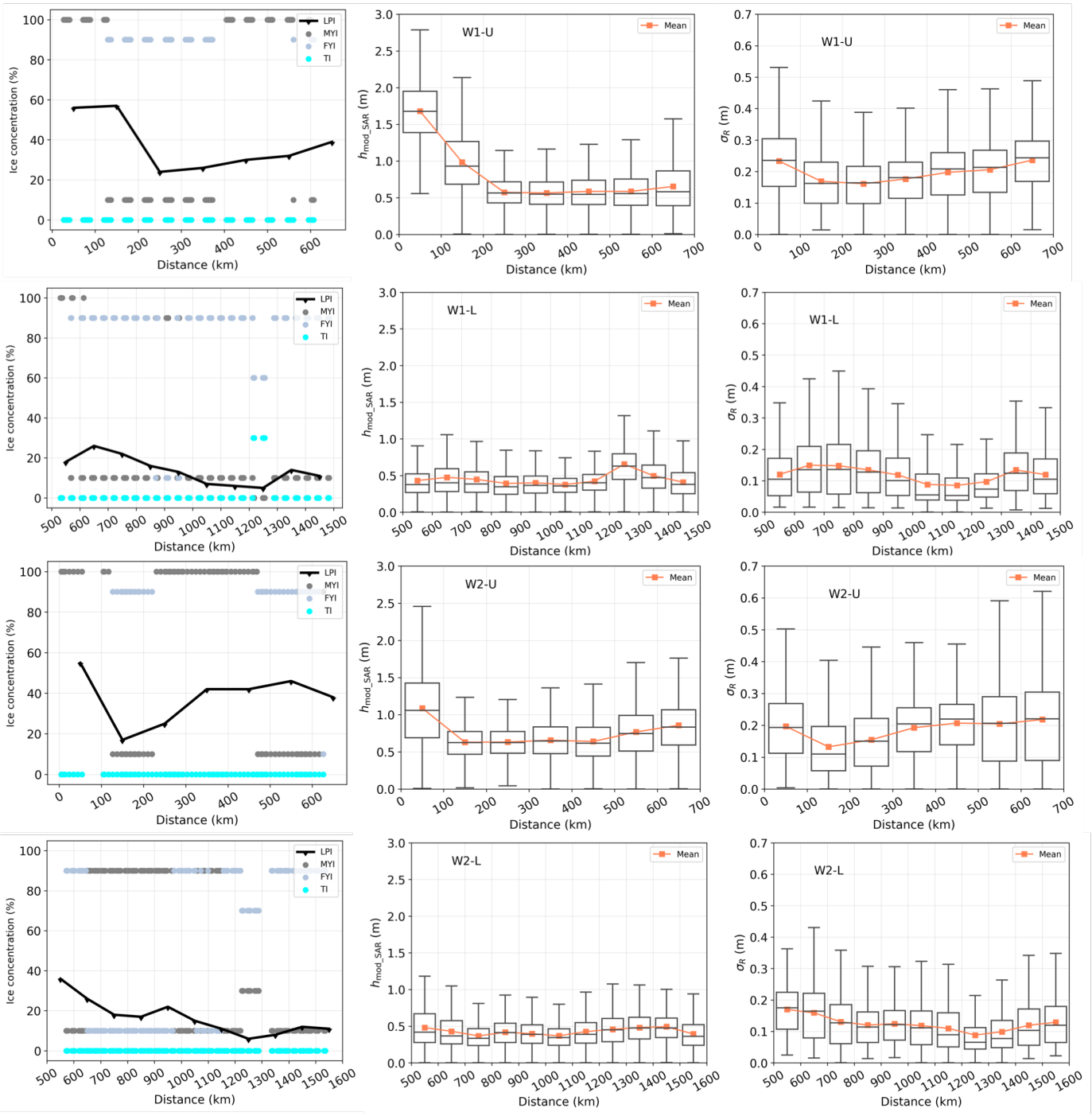

Fig. 4: Sea ice characteristics along the southwards direction along W1 and W2 segments. The blue line in the first column displays the OI percentages derived from SAR images, and the blue dot indicates the ice types obtained from the Ice Charts. The second and third columns plot the elevation ($h_{\mathrm{mod\_SAR}}$) and roughness (σ_R), respectively. Distance is measured from the northernmost SAR image reference point towards the south. The orange line denotes the average values of $h_{\mathrm{mod_SAR}}$ and σ_R. The box's upper and lower boundaries represent the first (Q1) and third (Q3) quartiles, while the upper (lower) whisker extends to the last (first) sample outside of Q3 $\pm 1.5\times$(Q3-Q1).

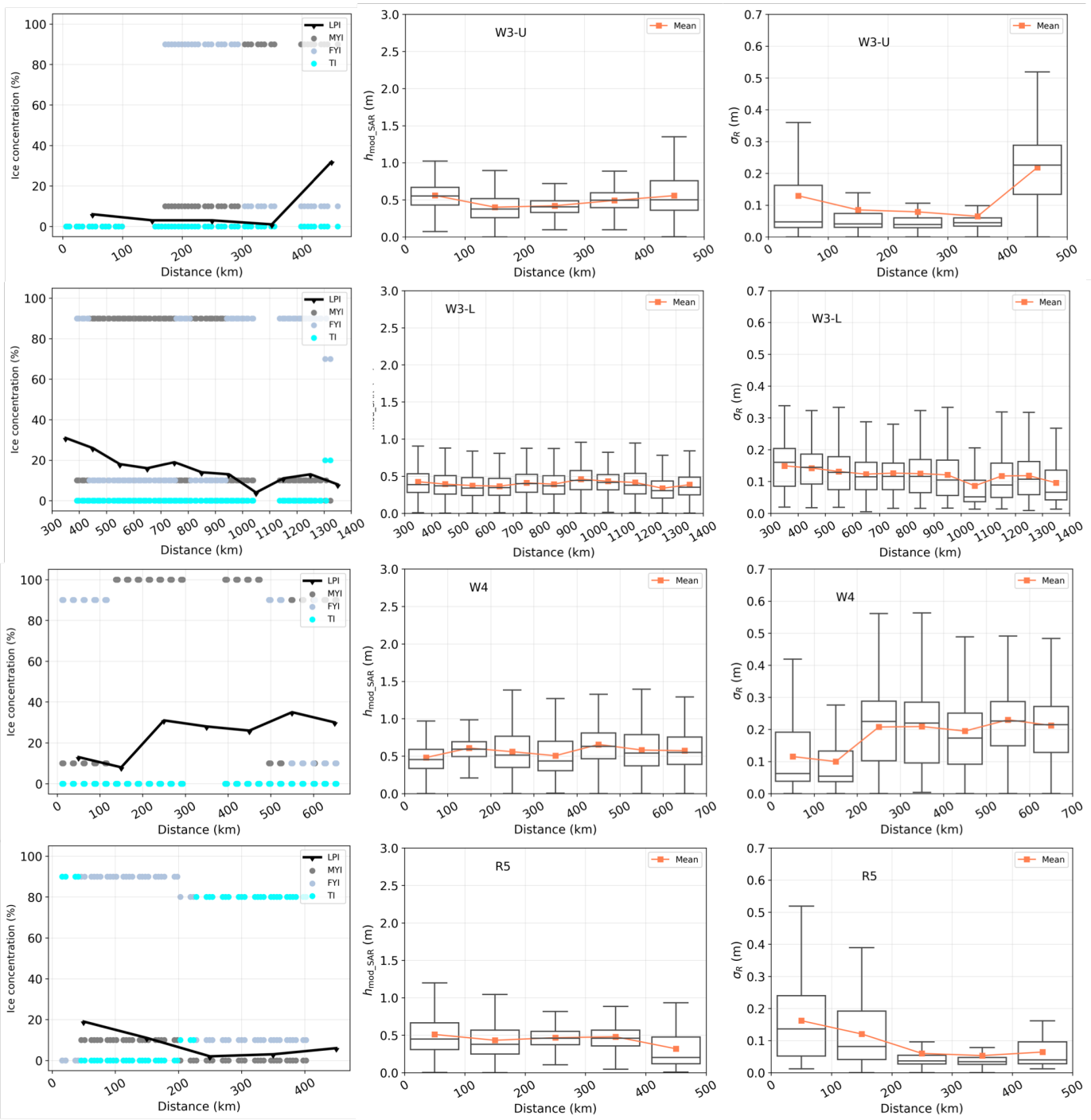

Fig. 5: Sea ice characteristics along the southwards direction along W3, W4, and R5 segments. The blue line in the first column displays the OI percentages derived from SAR images, and the blue dot indicates the ice types obtained from the Ice Charts. The second and third columns plot the elevation ($h_{\mathrm{mod\_SAR}}$) and roughness (σ_R), respectively.

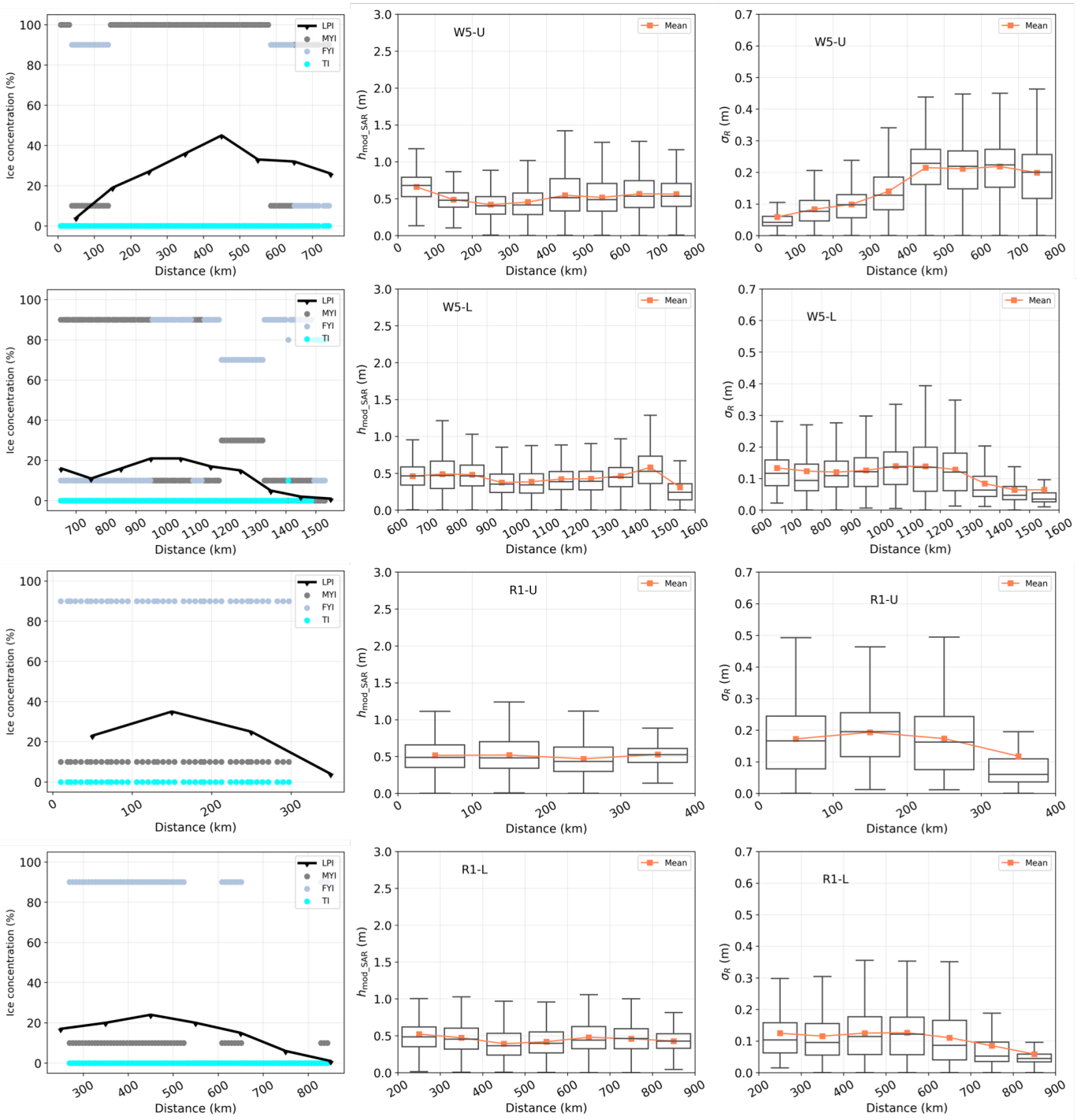

Fig. 6: Sea ice characteristics along the southwards direction along W5 and R1 segments. The blue line in the first column displays the OI percentages derived from SAR images, and the blue dot indicates the ice types obtained from the Ice Charts. The second and third columns plot the elevation ($h_{\mathrm{mod\_SAR}}$) and roughness (σ_R), respectively.

Q16: *R2 "… a digital …" or "digital elevation models"*
A16: Done

Q17: *R2-3 should it be drifting sea ice instead of drift sea ice?*
A17: Done

Q18: *R60-61. "sea ice elevation" has already been defined earlier in the manuscript.*

A18: The repeated statement has been removed.

Q19: *R76. With sequence is it meant orbit?*

A19: Yes, it means a series of acquisitions within some seconds along the same orbit. We revised the sentence: The footprints consist of 12 segments, each corresponding to a sequence of SAR images within the same orbit, all acquired at nearly the same time, with only seconds varying between them.

Q20: *R143. Wakabayashi et al 2004 used L-band SAR, how will this compare to the X-band SAR used here? Can we derive sea ice thickness using X-band SAR?*

A20: The work (Wakabayashi et al 2004) suggests that the co-polarization ratio from L-band SAR image has been demonstrated related to ice-thickness. However, as far as we know, no published results demonstrate a relation between the co-polarization ratio from X-band SAR and ice-thickness. Nevertheless, the co-polarization coherence from TerraSAR-X has been demonstrated to be correlated to ice thickness over multi-year sea ice (Kim et al., 2011). This reference was cited in Section 2.6.3.

Kim, J.-W., Kim, D.-j., and Hwang, B. J.: Characterization of Arctic sea ice thickness using high-resolution spaceborne polarimetric SAR data, IEEE Trans. Geosci. Remote Sens., 50, 13–22, https://doi.org/10.1109/TGRS.2011.2160070, 2011.

In the revision, we clarified that the reference is based on L-band SAR data:

R_{coPol} extracted from L-band SAR images, which is related to the dielectric constant, has been considered as an indicator of ice thickness (Wakabayashi et al., 2004). Further investigation is required to determine if R_{coPol} from the X-band can also serve as a proxy for ice thickness.

Q21: *R198. The reference can be shortened to (Meier, Markus and Comiso, 2018)*

A21: Done

Q22: *R248. "... in the Ice Charts"*

A22: Done

Q23: *R283. Sea ice doesn't evolve from MYI to TI. TI can evolve to MYI through surviving at least 2 seasonal cycles.*

A23: We refer to the spatial transition of sea ice types from MYI to TI in the southeastward direction.

We have revised the sentence as:

This observation aligns with the transition of ice types from MYI to TI in that direction.

Q24: *R363-367. It this information needed here?*

A24: We prefer to keep these sentences as a summary of our observations regarding sea ice DEMs. This enables readers who may skip the detailed reading of Sections 4.2 and 4.3 to still grasp some key take-home messages.

Again, we sincerely thank the editor and reviewers for helping us improving the manuscript.